Biosensors and Bioelectronics 26 (2011) 3832–3837

Contents lists available at ScienceDirect

Biosensors and Bioelectronics

journal homepage: www.elsevier.com/locate/bios

Integrated polymer-based Mach-Zehnder interferometer label-free streptavidin biosensor compatible with injection molding

R. Bruck[a,*], E. Melnik[a], P. Muellner[a], R. Hainberger[a], M. Lämmerhofer[b]

[a] AIT Austrian Institute of Technology GmbH, Health & Environment, Nano Systems, Donau-City-Strasse 1, 1220 Vienna, Austria
[b] Department of Analytical Chemistry, University of Vienna, Waehringer Strasse 38, 1090 Vienna, Austria

ARTICLE INFO

Article history:
Received 22 December 2010
Received in revised form 18 February 2011
Accepted 24 February 2011
Available online 3 March 2011

Keywords:
Mach-Zehnder interferometer
Polymer waveguide
Biosensor
Streptavidin
Polyimide
Label-free
Injection molding

ABSTRACT

We report the development of a Mach-Zehnder interferometer biosensor based on a high index contrast polymer material system and the demonstration of label-free online measurement of biotin–streptavidin binding on the sensor surface. The surface of the polyimide waveguide core layer was functionalized with 3-mercaptopropyl trimethoxy silane and malemide tagged biotin. Several concentrations of Chromeon 642-streptavidin dissolved in phosphate buffered saline solution were rinsed over the functionalized sensor surface by means of a fluidic system and the biotin-streptavidin binding process was observed in the output signal of the interferometer at a wavelength of 1310 nm. Despite the large wavelength and the comparatively low surface sensitivity of the sensor system due to the low index contrast in polymer material systems compared to inorganic material systems, we were able to resolve streptavidin concentrations of down to 0.1 μg/ml. The polymer-based optical sensor design is fully compatible with cost-efficient mass production technologies such as injection molding and spin coating, which makes it an attractive alternative to inorganic optical sensors.

1. Introduction

Currently, most clinical diagnostic tests are laborious and require sophisticated equipment operated by specially trained staff, and are, therefore, expensive. These tests often involve time consuming labeling techniques that attach fluorescent or radioactive markers on the analytes to be measured. Integrated optical biosensors, in particular those based on the evanescent wave principle, in combination with microfluidic systems represent a promising way to overcome these disadvantages and allow affordable point of care diagnostic systems. Fig. 1a shows a sketch of the evanescent wave sensing principle. Such integrated evanescent wave biosensors not only offer rapid and online detection of binding events on the sensor surface but also provide high sensitivity for the direct and label-free measurement of biomolecular interactions (Lechuga, 2005). Due to the small device footprint of such integrated devices, arrays of sensors can be combined in a single fluidic package, allowing the parallel detection of multiple analytes while keeping the sample volume consumption low. Because of hygienic standards and to prevent cross contaminations, the sensors including the fluidic system have to be designed as a single use system. Therefore, fabrication costs are another critical parameter.

Our research activities target at the realization of disposable all-polymer optical sensor chips for the label-free detection of biomolecules (Bruck and Hainberger, 2008) employing evanescent sensing in an integrated Mach-Zehnder interferometer (MZI) configuration (Heideman et al., 1993; Heidemann et al., 1996; Prieto et al., 2003). Evanescent sensing devices for biosensing have been proposed and demonstrated in various configurations, e.g. as grating sensors in titanium dioxide (Tiefenthaler and Lukosz, 1988), as MZIs in silicon oxynitride (Brosinger et al., 1997) or as ring resonators in SOI (De Vos et al., 2007; Bailey et al., 2009; Wright et al., 2010). So far, such devices have mostly been realized in inorganic material systems (Fan et al., 2008; Mukundan et al., 2009), where the waveguides structures are fabricated using standard semiconductor technology.

The use of transparent polymers as optical waveguide materials has attracted great attention for a wide range of applications (Tung et al., 2005). Polymers provide tunable properties, and therefore, allow large flexibility on the design of optical elements. The processing of polymers is based on powerful technologies such as injection molding, hot embossing, and spin coating, which are suited for cost-effective mass production. Polymers in optics and photonics have become an important factor and a wide variety of applications have been demonstrated. Examples are polymer waveguide grating couplers (Waldhäusl et al., 1997), polymer arrayed waveguide gratings (Guo et al., 2002), and polymer waveguide amplifiers (Pun, 2005). In most polymer material systems, refractive index differences between core and cladding layers are

* Corresponding author. Tel.: +43 050550 4309; fax: +43 050550 4399.
E-mail address: roman.bruck@ait.ac.at (R. Bruck).

0956-5663/$ – see front matter © 2011 Elsevier B.V. All rights reserved.
doi:10.1016/j.bios.2011.02.042

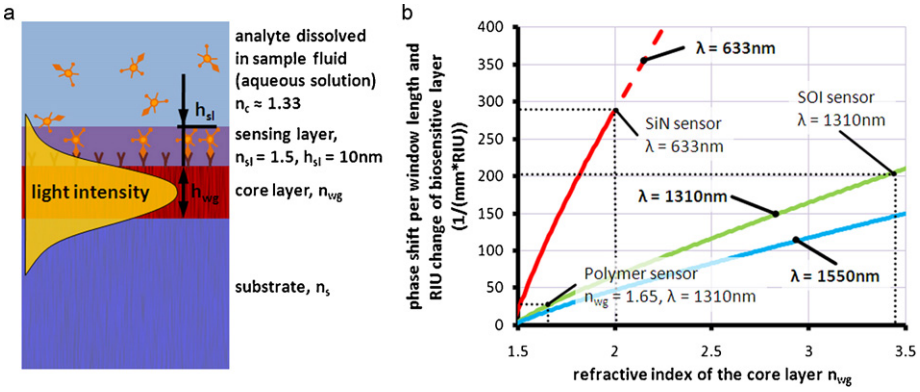

Fig. 1. (a) Principle of evanescent wave sensing for a slab waveguide. If the core layer thickness h_{wg} becomes sufficiently small, a certain amount of the guided light penetrates into the surrounding low index layers. If a thin biosensitive layer on top of the core layer changes its optical properties, i.e. thickness and/or refractive index, the effective index and, therefore, the propagation speed and the wavelength of the guided mode changes as well. When travelling over a fixed distance, the propagating wave accumulates a certain phase shift if the sensing layer changes. (b) Maximum phase shift that can be reached per millimeter length as function of the refractive index of the core layer, if an optimized waveguide geometry is used and if the sensing layer changes its refractive index by one refractive index unit (RIU), for the wavelengths 633 nm, 1310 nm and 1550 nm (TE-polarization).

in the range of a few tenths or a few hundredths, which leads to dimensions for single mode waveguide cross sections of several micrometers (e.g. Nordström et al., 2007; Paloczi et al., 2004; Tung et al., 2005). The devices presented in this paper are based on polyimide (PI, $n = 1.65$) for the waveguide core layer with an index difference of nearly 0.2 to the substrate. This is around one order of magnitude higher than typical polymer waveguide systems and, therefore, necessitates much smaller waveguide dimensions for single mode operation.

Our sensor design is based on the highly sensitive MZI. This sensor concept, realized with inorganic materials, has successfully been used for the detection of small concentrations of biomolecules. Such MZI biosensors have been realized for example with silicon nitride (SiN) rib waveguides (Schipper et al., 1997; Sepulveda et al., 2006; Zinoviev et al., 2008) or with SOI wire waveguides (Densmore et al., 2008). Polymer based integrated optical MZIs have been applied to bulk sensing (e.g. Bruck and Hainberger, 2008; Shew et al., 2005), and have been proposed for biosensing (Esinenco et al., 2005; Müllner et al., 2005). Shew et al. (2008) fabricated a MZI for biosensing applications based on inverted rib SU-8 waveguides. However, due to the very low index difference of only 0.004 and the large waveguide thickness of 6 μm it follows from theoretical considerations (sensitivity parameter defined by Parriaux and Veldhuis, 1998) that the fabricated sensor can have only a very little surface sensitivity. Demonstrations of biosensing employing polymer waveguide structures have, e.g. been reported utilizing polystyrene-wire ring resonators (Chao et al., 2006) or Bragg-grating sensors (Kim et al., 2010).

In this work, we demonstrate the measurement of the biotin–streptavidin binding process, which was chosen because of its well-known characteristics (e.g. Green, 1975; Weisser et al., 1999) and the wide range of published results that can be used for comparison.

The design of the sensor, where the low index substrate carries all necessary optical structures for the sensor, while the high index core layer and the low index cladding layer are applied by spin coating, is motivated by the possibility to transfer the sensor design on polymer substrates that are fabricated by injection molding or hot embossing, and therefore, take full advantage of the powerful technology platform that is available for polymer processing. In this paper, we present evanescent sensors based on single-mode polymer waveguides and with polymer cladding realized on silicon wafers with a 5 μm thick silicon dioxide (SiO_2) on top as substrates, which were patterned by well-known semiconductor fabrication processes. This allows testing of core and cladding polymer processing, the MZI sensor as well as optimizing the surface modification protocol for streptavidin binding without the need for polymer substrates.

Several issues have to be addressed when designing a polymer based evanescent wave sensor for surface sensing applications. First of all, the index difference between the substrate and the core layer is critical for maximizing the surface sensitivity. Compared to inorganic material systems such as SiN/SiO_2 or SOI, polymer material systems feature only a small index difference, which leads to a reduced surface sensitivity. Fig. 1b plots the maximum achievable phase shift per length of the sensing window and per refractive index change of the sensing layer as function of the core layer refractive index for the wavelengths 633 nm, 1310 nm and 1550 nm (TE-polarization). The highest sensor sensitivity is obtained for SiN waveguides ($n_{wg} = 2$, $h_{wg} = 75$ nm) at a wavelength of 633 nm. Silicon waveguides ($n_{wg} = 3.46$, $h_{wg} = 60$ nm), which are not transparent below 1100 nm, are typically operated at telecom wavelengths 1310 nm or 1550 nm and have about 25% lower sensitivity compared to SiN waveguides at 633 nm despite their higher refractive index. The sensitivity of the polymer material system ($n_{wg} = 1.65$, $h_{wg} = 350$ nm) investigated here at 1310 nm is nearly one order of magnitude smaller than SiN waveguides at 633 nm. However, we found that this disadvantage is partly compensated by the fact that a higher density of streptavidin molecules can be bound on the chosen polymer surface compared to silicon based surfaces. Xu et al. (2008) measured a maximum density of streptavidin on their SOI ring resonator sensor of about 25 fM/mm^2 (1.6 ng/mm^2), whereas we were able to verify with fluorescent measurements that the maximum streptavidin density on our polymer surface is around 144 fM/mm^2.

Moreover, physical and chemical properties of the polymers have to be taken into account. In our approach, it is necessary that the core layer polymer can be spin-coated as a homogeneous but very thin layer of about 350 nm in order to achieve maximum sensitivity. All used polymers have to withstand the chemical treatment that is necessary for the modification of the sensor surface for streptavidin sensing and have to be absolutely stable in the measurement environment.

2. Sensor fabrication and measurement setup

The MZI sensor chips were fabricated on silicon substrates covered with a 5 μm thick SiO_2 layer. The rib of the waveguide structures was patterned into the SiO_2 surface using conventional UV-lithography and an SF_6 reactive ion etching (RIE) process. The

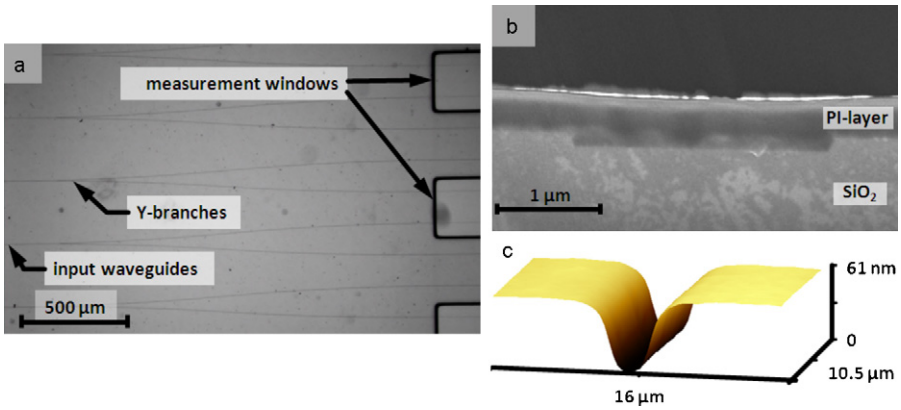

Fig. 2. (a) Microscope picture of MZI-array showing input waveguides of the MZIs that are split by means of Y-branches into the two arms of the interferometer as well as the beginning of the measurement windows. (b) SEM micrograph of a single mode inverted rib waveguide cross section with a spin coated PI layer, obtained from a cleaved sample end facet. (c) AFM scan of the PI surface above a waveguide trench with an etch depth of 150 nm. The surface modulation of the 450 nm thick PI layer is about one third of the etch depth of the waveguide trench in the SiO_2. The single mode behavior of the waveguides is not influenced by this modulation.

PI core layer was spin-coated with a thickness of 450 nm and, after activation with UV-light, thermally cured for 1 h at 200 °C. The waveguide trench etched into the SiO_2 surface is filled up with the high index core polymer in this spin-coating step and, thus, generates a rib waveguide structure. The inset in Fig. 3 depicts the waveguide cross section. The chosen PI thickness of about 450 nm reduces the surface sensitivity of the sensor by about 20% compared to the optimum thickness of 350 nm but was found to be necessary to suppress leakage into the silicon substrate through the 5 µm thick oxide layer. Ormoclad as 5 µm thick cladding was applied employing another spin-coating step. This layer was then exposed to UV-light, except for the 1 cm long measurement window over one arm of the interferometer, and developed in Ormodev for 1 min. Finally, this layer was thermally cured for 3 h at 150 °C. Fig. 2 shows a microscope picture of a MZI array on one of the fabricated samples together with a SEM micrograph of an inverted rib waveguide cross section as well as an AFM scan of the PI surface over a waveguide trench, which reveals a non-perfect planarization of the PI surface.

A surface modification protocol for the binding of biotin on the PI surface had to be developed and optimized for maximum streptavidin binding capacity, while not attacking the thin PI core layer. For the functionalization of the PI surface, the samples were first exposed to oxygen plasma for 1 min. The samples were then dipped into MPTMS solution (acetate buffer 0.07 M, 25%v methanol, 2.8%v TritonX-100 and 3%v 3-mercaptopropyl trimethoxy silane) for 1 h at room temperature. Finally, the samples were dipped at room temperature for 2 h into M-PEG_2-biotin solution (5 µM Malemide–PEG_2–biotin solved in ultrapure water with 10%v isopropanol and 10%v phosphate buffer). After the surface functionalization with biotin, the sensor surface was blocked with bovine serum albumin (BSA) by dipping the sensor chips for 30 min into phosphate buffered saline (PBS) buffer solution with 100 µg/ml BSA. Our measurements showed that the BSA blocking procedure reduces the measurement signal by about 40% but successfully suppresses non-specific binding of streptavidin on the modified PI surface.

Before the measurements, the samples were cleaved to provide a clean high-quality facet for end face coupling. After mounting of the samples on the measurement setup a polydimethylsiloxane (PDMS) flow chamber was attached to the sensor chip and connected to a syringe pump as well as to the sample fluid reservoirs. The light of a tunable laser source with a center wavelength of 1310 nm was guided to the sensor by means of a single mode fiber. The light is coupled from the single mode fiber into the PI waveguide by means of end face coupling. On the chip, a Y-branch splits the light into the two arms of the interferometer: the reference arm that is covered with a cladding and the sensing arm that gets in direct contact with the sample fluid for a length of 1 cm. After recombining the two arms again, the transmitted light is end-face coupled to a tapered lens fiber and then guided to an optical power meter. Fig. 3 schematically shows the measurement setup. The sensor chips were not temperature stabilized.

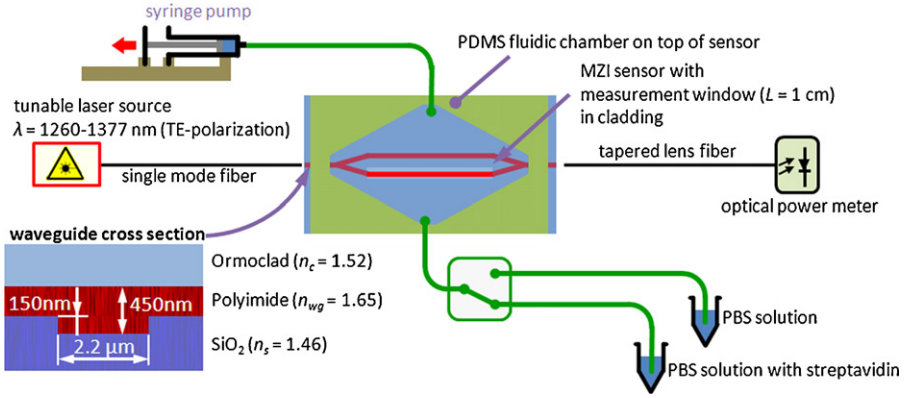

Fig. 3. Measurement setup: the light of a fiber-coupled tunable laser source is end-face coupled to the polyimide rib waveguide on the sensor chip. At the output of the sensor chip, the transmitted light is end-face coupled to a tapered lens fiber and then guided to an optical power meter. On top of the sensor chip a PDMS flow chamber is mounted, which allows rinsing different solutions over the sensing arm of the MZI.

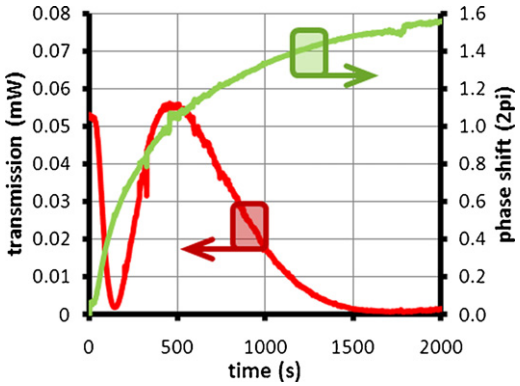

Fig. 4. Transmitted power and calculated phase shift of a MZI sensor during the detection of 10 μg/ml streptavidin dissolved in PBS solution. The ratio between the maximum and the minimum transmission of the MZI sensor is higher than 15 dB.

3. Results and discussion

In the measurements, the sensor surface was first rinsed with a 150 mM PBS solution (pH 7.2) at a flow rate of 20 μl/min, which corresponds to an average flow speed of about 2.5 cm/min. This allowed verifying the stability of the sensor signal. Then we introduced different concentrations of Chromeon 642-streptavidin ranging from 25 μg/ml down to 0.1 μg/ml dissolved in PBS at a flow rate of 20 μl/min to the sensor surface. Each measurement was performed on a separate sample. Fig. 4 plots the transmitted power of the MZI sensor during the measurement of 10 μg/ml streptavidin in PBS solution. At the beginning of the measurement we adjusted the wavelength of our tunable laser light source to a point where the MZI showed maximum transmission. Although this point does not show maximum sensitivity for small changes of the effective index of the propagating mode, it simplifies the calculation of the phase shift out of the sensor transmission. Then, we introduced the streptavidin containing buffer to the sensor surface and recorded the change in the transmission of the MZI sensor as function of time. From this data we calculated the accumulated phase shift during this measurement by reversing the sinusoidal characteristic of the MZI. The calculated phase shift for this measurement is given in the same diagram as the transmitted power in Fig. 4. Finally, we rinsed PBS solution without streptavidin with the same flow rate over the sensor surface. We found that during rinsing no change in the accumulated phase shift arises, which means that no significant amount of bound streptavidin is washed away. For this measurement the insertion loss from the laser source to the photo detector is better than −18 dB. The ratio between maximum and minimum transmitted power of the MZI is larger than 15 dB. Repeated measurements of the same streptavidin concentration on different samples indicate that the standard deviation of our measurements is around 12%. On the basis of the assumption that the core layer thickness varies from sample to sample by ±25 nm due to variations in the spin coating process, calculations showed that the induced phase shift of the sensor can change by about ±5%. The remaining deviations can be attributed to variations of the biotin density on the sensor surface after surface modification.

Similar measurements were performed for different concentrations of streptavidin in PBS solution ranging from 25 μg/ml down to 0.1 μg/ml. Fig. 5 summarizes these measurements. As expected, the higher the streptavidin concentration, the larger the induced phase shift in the interferometer. The steps in the measurement curves (e.g. curve for 25 μg/ml at a time of 1750 s or curve for 1 μg/ml at a time of 850 s) are caused by the correction of a misalignment of the input or output fiber. The setup suffers from a slow mechanical drift, which is corrected intentionally by activating the fiber auto alignment system. The automatic switching of the optical power meter between different measurement ranges can also result in dips or peaks in the measurement curves, e.g. in the curve for 10 μg/ml at a time of 330 s or curve for 0.5 μg/ml at a time of 1150 s.

Fig. 6 plots the measured phase shift as a function of the streptavidin concentration for fixed times of 200 s, 500 s, and 1000s. For the lowest concentration of 0.1 μg/ml streptavidin, the phase shift is $0.007 \times 2\pi$ at $t = 200$ s, $0.028 \times 2\pi$ at $t = 500$ s and $0.0549 \times 2\pi$ at $t = 1000$s. In order to facilitate measurements of low concentrations with small resulting phase shifts it is beneficial to start close to a point of minimum transmission by adjusting the wavelength of the laser source. If the transmitted power is measured on a linear scale, the most sensitive point of the MZI for small changes of the effective mode index is the so-called quadrature point, where the MZI transmit half of the maximum power. When measuring on a logarithmic scale the points of maximum sensitivity are shifted towards the transmission minimum. The higher the extinction ratio, the higher is the maximum sensitivity and the closer are the points of maximum sensitivity to the transmission minimum. Keeping that in

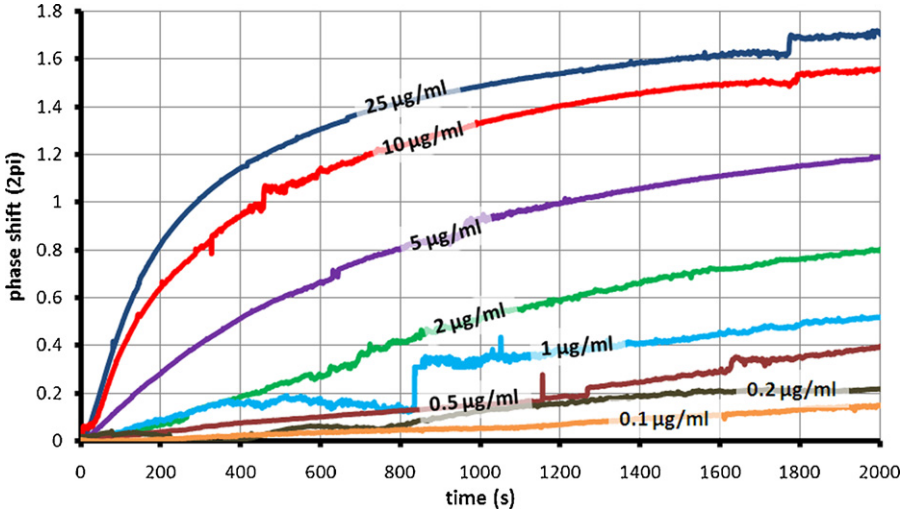

Fig. 5. Measured phase shift as function of time for different streptavidin concentrations in PBS solution. The steps in the measurement curves (e.g. curve for 25 μg/ml at a time of 1750 s or curve for 1 μg/ml at a time of 850 s) are caused by the correction of a misalignment of the input or output fiber. The setup suffers from a slow mechanical drift, which is corrected intentionally by activating the fiber auto alignment system. The automatic switching of the optical power meter between different measurement ranges can also result in dips or peaks in the measurement curves, e.g. in the curve for 10 μg/ml at a time of 330 s or curve for 0.5 μg/ml at a time of 1150 s.

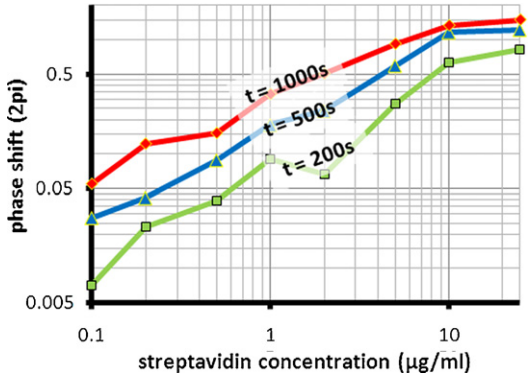

Fig. 6. Phase shift as function of the streptavidin concentration measured at 200 s, 500 s and 1000s.

mind and assuming a ratio of 15 dB between the minimum and maximum transmission of the MZI, the given phase shifts translate to a change in the transmission by nearly 1 dB for $t = 500$ s and nearly 3 dB for 1000 s, which can be resolved easily.

We verified that unspecific binding of streptavidin on the PI surface can be blocked employing BSA. For this purpose we prepared the sensor surface by exposing it to oxygen plasma and MPTMS solution but without dipping into M-PEG_2–biotin solution. After blocking of the MPTMS functionalized surface with BSA we rinsed PBS buffer with and without streptavidin over the sensor surface. The small observed response was caused by the slightly different bulk refractive index of the PBS solution with streptavidin and could be fully reversed by rinsing the sensor again with pure PBS. Comparing the results of the sensors with and without BSA blocked surfaces revealed that the total binding capacity of streptavidin and, therefore, the maximum achievable phase shift during a measurement is reduced by about 40% when using a BSA blocked surface. From these results we conclude that without BSA blocking 40% of the sensor response is induced by non-specific binding of streptavidin on the PI surface. In contrast to BSA blocked samples, where rinsing with PBS after the streptavidin binding process does not result in a reduction of the phase shift, rinsing with PBS solution after the measurement on non-blocked samples reduces the phase shift by about 10% because weakly bound streptavidin is washed away.

The biotin–streptavidin system is commonly used to demonstrate the performance of optical biosensors and highly sensitive devices have been demonstrated. Examples are sub-nM detection of streptavidin with ring resonators in the most sensitive SiO_2/SiN material system at a wavelength of 633 nm (Ksendzov and Lin, 2005) or the detection of 60 fM streptavidin with a SOI ring resonator array (Iqbal et al., 2010). Due to the comparatively low refractive index contrast our polymer based sensor cannot compete with these demonstrations in terms of sensitivity. However, our approach is fully compatible with low-cost mass-production technologies, which makes it attractive as disposable sensor for applications where ultra-high sensitivity is not required and fabrication costs are a driving factor. It also has to be mentioned that depending on the instrumental effort the achievable sensitivity of SOI based sensing devices can be significantly lower than that of the above cited systems. For instance, the smallest measured streptavidin concentrations reported in recent publications employing SOI ring resonators are in the range of 0.1 μg/ml (Xu et al., 2008) and 1 μg/ml (Bienstmann et al., 2009), which is similar to our results. Comparing our results with publications of other polymer based biosensors, a considerable improvement in the smallest measurable streptavidin concentration is obvious. The smallest concentration measured by Chao et al. (2006) employing polystyrene-wire ring resonators was 1 μM, whereas Kim et al. (2010) measured 33.2 nM utilizing Bragg-grating sensors. Our smallest concentration measured of 0.1 μg/ml translates to 1.66 nM, which is an enhancement of more than one order of magnitude compared to Kim et al., and nearly three orders of magnitude compared to Chao et al.

4. Conclusion and outlook

We demonstrated sensor chips for biosensing employing an integrated Mach-Zehnder interferometer with single mode polymer rib waveguides. The sensor utilizes a high refractive index polyimide ($n = 1.65$) as waveguide core layer. We developed an optimized surface modification protocol for immobilization of biotin on the polyimide surface. Experimental results on real-time measurements of Chromeon 642-streptavidin binding on the sensor surface show that a streptavidin concentration as low as 0.1 μg/ml (= 1.66 nM) can be detected. The theoretical sensitivity of the sensor can be improved by a factor of four by changing the wavelength to 633 nm and adopting the waveguide cross sections to the shorter wavelength. Despite the comparatively low theoretical surface sensitivity due to the low refractive index contrast and the large wavelength of 1310 nm used, the experimental results match that of several recent publications on SOI platforms. We attribute this fact to the high streptavidin binding capacity of the modified polyimide surface. In principle, the reported sensor design can be directly transferred to injection molded polymer substrates that carry all necessary optical waveguide structures. This would allow for mass production of MZI sensor chips at very low costs.

A suitable polymer for the realization of injection molded substrates is polymethylpentene (PMP, $n = 1.46$), which matches the refractive index of SiO_2. Preliminary results on the injection molding of photonic structures in PMP as well as first waveguiding experiments confirming the process compatibility of the material system presented in this paper with PMP substrates have already been published elsewhere (Bruck et al., 2010). The realization of a MZI structure on injection molded substrates was so far prevented by high losses in single mode waveguides arising from imperfect replication of the waveguide structures. The improvement of single mode waveguide transmission necessitates advancements in the injection molding process and is subject of ongoing research. However, it has to be admitted that for the final device there is no experience on how the reduced mechanical stiffness or the higher thermal expansion of the polymer substrate affect the stability of the sensor signal.

Acknowledgements

The authors want to thank Nadezhda Kataeva for her support with the AFM and the SEM. This work was supported by the Austrian NANO Initiative under the grants PLATON PolyWaG (project no. 1152) and PolyIMPD (project no. 819659).

References

Bailey, R.C., Washburn, A.L., Qavi, A.J., Iqbal, M., Gleeson, M., Tybor, F., Gunn, L.C., 2009. Proc. SPIE 7220, 72200N–72201N.
Bienstmann, P., De Vos, K., Claes, T., Debackere, P., Baets, R., Girones, J., Schacht, E., 2009. Proc. SPIE 7220, 72200O.
Brosinger, F., Freimuth, H., Lacher, M., Ehrfeld, W., Gedig, E., Katerkamp, A., Spener, F., Cammann, K., 1997. Sens. Actuators B Chem. 44, 350–355.
Bruck, R., Hainberger, R., 2008. Proc. SPIE 7138, 71380N.
Bruck, R., Hainberger, R., Heer, R., Kataeva, N., Köck, A., Krapf-Günther, M., Kaiblinger, K., Pipelka, F., Bilenberg, B., 2010. Proc. SPIE 7788, 77880A.
Chao, C.Y., Fung, W., Guo, L.J., 2006. IEEE J. Sel. Top. Quantum Electron. 12, 134–142.
De Vos, K., Bartolozzi, I., Schacht, E., Bienstman, P., Baets, R., 2007. Opt. Exp. 15, 7610–7615.
Densmore, A., Xu, D.X., Janz, S., Waldron, P., Mischki, T., Lopinski, G., Delage, A., Lapointe, J., Cheben, P., Lamontagne, B., Schmid, J.H., 2008. Opt. Lett. 33, 596–598.
Esinenco, D., Psoma, S.D., Kusko, M., Schneider, A., Muller, R., 2005. Rev. Adv. Mater. Sci. 10, 295.

Fan, X., White, I.M., Shopova, S.I., Zhu, H., Suter, J.D., Sun, Y., 2008. Anal. Chim. Acta 620, 8–26.
Green, N.M., 1975. Adv. Protein Chem. 29, 85–133.
Guo, W.E., Ma, C.S., Zhang, D.M., Chen, K.X., Zhao, Y., Cui, Z.C., Liu, S.Y., 2002. Opt. Commun. 201, 45–53.
Heideman, R.G., Kooyman, R.P.H., Greve, J., 1993. Sens. Actuators B Chem. 10, 209–217.
Heidemann, R.G., Veldhuis, G.J., Jager, E.W.H., Lambeck, P.V., 1996. Sens. Actuators B Chem. 35, 234.
Iqbal, M., Gleeson, M.A., Spaugh, B., Tybor, F., Gunn, W.G., Hochberg, M., Baehr-Jones, T., Bailey, R.C., Gunn, L.C., 2010. IEEE J. Sel. Top. Quantum Electron. 16, 654–661.
Kim, J.W., Kim, K.J., Yi, J.A., Oh, M.C., 2010. IEEE J. Sel. Top. Quantum Electron. 16, 973–980.
Ksendzov, A., Lin, Y., 2005. Opt. Lett. 30, 3344–3346 (IEEE J. Sel. Top. Quantum Electron. 16, 654–661).
Lechuga, L.M., 2005. In: Gorton, L. (Ed.), Biosensors and Modern Biospecific Analytical Techniques. Elsevier Science BV, Amsterdam, pp. 209–250.
Mukundan, H., Anderson, A.S., Grace, W.K., Grace, K.M., Hartman, N., Martinez, J.S., Swanson, B.I., 2009. Sensors 9, 5783–5809.
Müllner, R., Obreja, P., Kusko, M., Esinenco, D., Tibeica, C., Conache, G., Buia, L., Apostol, D., Damian, V., Mateescu, M., Diaconu, M., Moldovan, L., 2005. Proc. SPIE 5972.
Nordström, M., Zauner, D.A., Boisen, A., Hübner, J., 2007. J. Lightwave Technol. 25, 1284–1289.
Paloczi, G.T., Huang, Y., Yariv, A., 2004. Appl. Phys. Lett. 85, 1662–1664.
Parriaux, O., Veldhuis, G.J., 1998. J. Lightwave Technol. 16, 573–582.
Prieto, F., Sepulveda, B., Calle, A., Llobera, A., Domınguez, C., Abad, A., Montoya, A., Lechuga, L.M., 2003. Nanotechnology 14, 907.
Pun, E.Y.B., 2005. ICTON, Tu.B2.3.
Schipper, E.F., Brugman, A.M., Dominguez, C., Lechuga, L.M., Kooyman, R.P.H., Greve, J., 1997. Sens. Actuators B Chem. 40, 147–153.
Sepulveda, B., Sanchez del Rıo, J., Moreno, M., Blanco, F.J., Mayora, K., Domınguez, C., Lechuga, L.M., 2006. J. Opt. A: Pure Appl. Opt. 8, 561–566.
Shew, B.Y., Kuo, C.H., Huang, Y.C., Tsai, Y.H., 2005. Sens. Actuators A Phys. 120, 383–389.
Shew, B.Y., Cheng, Y.C., Tsai, Y.H., 2008. Sens. Actuators A Phys. 141, 299–306.
Tiefenthaler, K., Lukosz, W., 1988. J. Opt. Soc. Am. B 6, 209–220.
Tung, K.K., Wong, W.H., Pun, E.Y.B., 2005. Appl. Phys. A 80, 621–625.
Waldhäusl, R., Schnabel, B., Dannberg, P., Kley, E., Bräuer, A., Karthe, W., 1997. Appl. Opt. 36, 9383.
Weisser, M., Tovar, G., Mittler-Neher, S., Knoll, W., Brosinger, F., Freimuth, H., Lacher, M., Ehrfeld, W., 1999. Biosens. Bioeletron. 14, 405–411.
Wright, J.B., Brener, I., Westlake, K.R., Branch, D.W., Shaw, M.J., Vawter, G.A., 2010. Proc. SPIE 7605, 76050C–76051C.
Xu, D.X., Densmore, A., Delâge, A., Waldron, P., McKinnon, R., Janz, S., Lapointe, J., Lopinski, G., Mischki, T., Post, E., Cheben, P., Schmid, J.H., 2008. Opt. Exp. 16, 15137–15147.
Zinoviev, K., Carrascosa, L.G., Sanchez del Rio, J., Sepulveda, B., Dominguez, C., Lechuga, L.M., 2008. Adv. Opt. Tech. 2008, 383927.